Supplemental Document

Shadow of a laser beam: supplement

Raphael A. Abrahao,[1,2,*] Henri P. N. Morin,[1,3] Jordan T. R. Pagé,[1,4] Akbar Safari,[1,5] Robert W. Boyd,[1,4,6] and Jeff S. Lundeen[1,7,8]

[1]*Department of Physics, University of Ottawa, 25 Templeton Street, Ottawa, Ontario, K1N 6N5, Canada*
[2]*Brookhaven National Laboratory, Upton, New York, 11973, USA*
[3]*Institute for Quantum Computing, Department of Physics and Astronomy, University of Waterloo, Waterloo, Ontario, N2L 3G1, Canada*
[4]*School of Electrical Engineering and Computer Science, University of Ottawa, Ottawa, Ontario, K1N 6N5, Canada*
[5]*Department of Physics, University of Wisconsin-Madison, Madison, Wisconsin, 53706, USA*
[6]*Institute of Optics, University of Rochester, Rochester, New York 14627, USA*
[7]*Joint Centre for Extreme Photonics, University of Ottawa - National Research Council of Canada, 100 Sussex Drive, Ottawa, Ontario K1A 0R6, Canada*
[8]*jlundeen@uottawa.ca*
[*]*rakelabra@bnl.gov*

This supplement published with Optica Publishing Group on 14 November 2024 by The Authors under the terms of the Creative Commons Attribution 4.0 License in the format provided by the authors and unedited. Further distribution of this work must maintain attribution to the author(s) and the published article's title, journal citation, and DOI.

Supplement DOI: https://doi.org/10.6084/m9.figshare.27144000

Parent Article DOI: https://doi.org/10.1364/OPTICA.534596

The shadow of a laser beam: supplemental document

1. METHODS

The analysis begins with the images taken from the scientific CMOS camera, taken at the maximum resolution of 3088 x 2076 pixels. The images are cropped to the ruby, keeping the resolution but reducing the size of the image to only the relevant part of the image. Several datasets are collected. A background set was collected with only the illuminating blue laser, to be used as the reference for all other powers. Datasets were taken with the green object laser at several power values. Each dataset comprises of 21 total images. This is obtained from the movement of the translation stage during data collection (total 2 mm displacement in steps of 0.1 mm in the y dimension). Each individual dataset is averaged into a single image. We integrate over the z dimension in each image. The result of this integration is mathematically described in Eq. S7. The position of the local minimum in the graph of the transmittance of the blue laser is determined. The maximum value obtained at this position is obtained through the background result. Combined, these two values are used to compute the contrast for that power of the green object laser.

The calculation of the contrast is discussed in the next paragraph. Since the normalization used is based on an experimental parameter, i.e., the background image when the green laser was off, it can happen that for some values the error bars cross the value of 1.0 of transmittance for a given reference value. However transmittance above 1.0 is meaningless. This issue is more relevant for low powers of the green laser.

2. THEORETICAL SIMULATIONS

A. Deriving the Model

The laser shadow effect is modeled through the use of rate equations for the populations of the Cr^{3+} ions in ruby. Let N be the total number density of ions in the ruby, N_1 the number density in the $|1\rangle = |^4A_2\rangle$ state, and N_3 the number density in the $|3\rangle = |^2E\rangle$ state. The lifetimes of the $|2\rangle = |^4T_2\rangle$ and $|4\rangle = |^2T_1\rangle$ are negligible and can be neglected. The total population is therefore:

$$N = N_1 + N_3. \tag{S1}$$

Hence, the population in the N_1 state is given by:

$$\frac{dN_1}{dt} = -\frac{I}{\hbar\omega}\sigma_1 N_1 + \frac{N_3}{T_3}, \tag{S2}$$

where σ_1 is the absorption cross-section of the first transition for the 532 nm object laser, T_3 is the lifetime of the metastable $|3\rangle$ state, I is the intensity of the 532 nm object laser, $\hbar$ is the reduced Planck constant, and ω is the angular frequency of the 532 nm object laser. We define the saturation intensity as:

$$I_S = \frac{\hbar\omega}{T_3\sigma_1}. \tag{S3}$$

We solve Eq. S2 at steady state ($\frac{dN_1}{dt} = 0$) condition. Eliminating N_3 from the solution gives us:

$$N_1 = \frac{N}{1 + 1/I_S}. \tag{S4}$$

From the definition of the absorption cross-section, we can write:

$$\alpha^{\text{blue}}(I) = \sigma_1^{\text{blue}} N_1 + \sigma_3^{\text{blue}} N_3. \tag{S5}$$

Using Equations S1 and S4, Equation S5 is simplified to only contain the total number density N. We then obtain an expression for the absorption of the illuminating blue laser as a function of the intensity of the green object laser:

$$\alpha^{\text{blue}}(I) = \frac{\sigma_1^{\text{blue}} N}{1 + I\frac{\sigma_1^{\text{green}} T_3}{\hbar\omega}} + \sigma_3^{\text{blue}} N \left(1 - \frac{1}{1 + I\frac{\sigma_1^{\text{green}} T_3}{\hbar\omega}}\right) \tag{S6}$$

This expression is then integrated over the z dimension to obtain:

$$I(y) = I_0 e^{-\int_0^L \alpha^{\text{blue}}(y,z)\mathrm{d}z}. \tag{S7}$$

where L is the length of the ruby crystal and I_0 is the background intensity. This equation is our model of the effect.

B. Using the Model

Several parameters need to be experimentally obtained to evaluate Eq. S7. These include: the beam waists w_{0x} and w_{0y} of the green laser (acting as the illuminated object), N the number density of the Cr^{3+} ions in the ruby, σ_1^{blue} and σ_1^{green}, the absorption cross-sections of both laser beams for the first transition, and σ_3^{blue} the absorption cross-section of the illuminating blue laser for the second transition. The lifetime T_3 will be used as a fit parameter.

The beam waists were experimentally determined using the razor blade method. For these measurements, the blade was ~ 10 mm away from the ruby in the x dimension and ~ 20 mm in the y dimension. The uncertainties attributed are the errors on the fit. We measured: $w_{0x} = 3.17 \pm 0.01$ mm and $w_{0y} = 0.168 \pm 0.003$ mm.

To obtain values for the absorption cross-sections for the first transition, we use Beer's Law:

$$T_j = e^{-\sigma_1^j N L}, \tag{S8}$$

where T_j is the transmission of the jth wavelength through the ruby, σ_1^j is the absorption cross-section for the first transition for the jth wavelength, N is the total number density of Cr^{3+} ions in the ruby, and L is the length of the ruby. The length was measured at $L = 12.0 \pm 0.5$ mm in both the z and x dimensions. To evaluate Eq. S8, we need to measure T_j.

Transmission values were obtained in the linear regime for both wavelengths. For the 450 nm illumination laser, the average power at the ruby was 285 μW. To measure the transmission of the green laser (532 nm, object laser), we set the green laser to a low power such that the average power reaching the cube was measured to be 934 μW. For both cases, transmission data was obtained by measuring the power before and after the ruby over 10 minutes, in the respective propagation path. The 450 nm illumination laser was allowed to stabilize for 5 hours before taking measurements. This raw data is then Fresnel corrected, using $n_{\text{ruby}} = 1.77$ and $n_{\text{air}} = 1.0003$. Errors are obtained by taking the standard deviation of the measurements. We obtain $T_{\text{blue}} = 26.01 \pm 0.02\%$ and $T_{\text{green}} = 26.8 \pm 0.3\%$. Thus these values are used to solve Eq. S8 simultaneously for σ_1 for both wavelengths.

Fitting the model against the experimental data allowed us to set the remaining three (3) unknowns, which are the total number density N, the absorption cross-section for the second transition for the 450 nm illumination laser σ_3^{blue}, and the lifetime T_3. We obtained $N = 2.5 \times 10^{25}$ m^{-3} and $\sigma_3^{\text{blue}} = 17.2 \times 10^{-24}$ m^2. The uncertainty on both of these values was set at $\pm 10\%$ as reported in Ref. [1]. The initial value of the metastable state's lifetime T_3 was initially set at $T_3 = 3$ ms, per the literature [2]. However, due to the temperature increase of the ruby, this value proved to be inaccurate and was reduced to $T_3 = 1$ ms.

C. Obtaining the Uncertainty Bands

The theoretical error bands as presented in Fig. 3 of the main text are determined as follows. The center theory curve is calculated using the mean values of all respective parameters. The model is then computed taking the extreme values of each parameter, individually. This allows us to isolate the effect of changing only a single parameter on the model. We take note at which parameters increase and which decrease the minimum value of the curve. The errors are then normalized in the same manner as previously indicated. All parameters which increase (decrease) the value of the minimum are added in quadrature. These values are then added (subtracted) from the central theory curve to obtain the error bands.

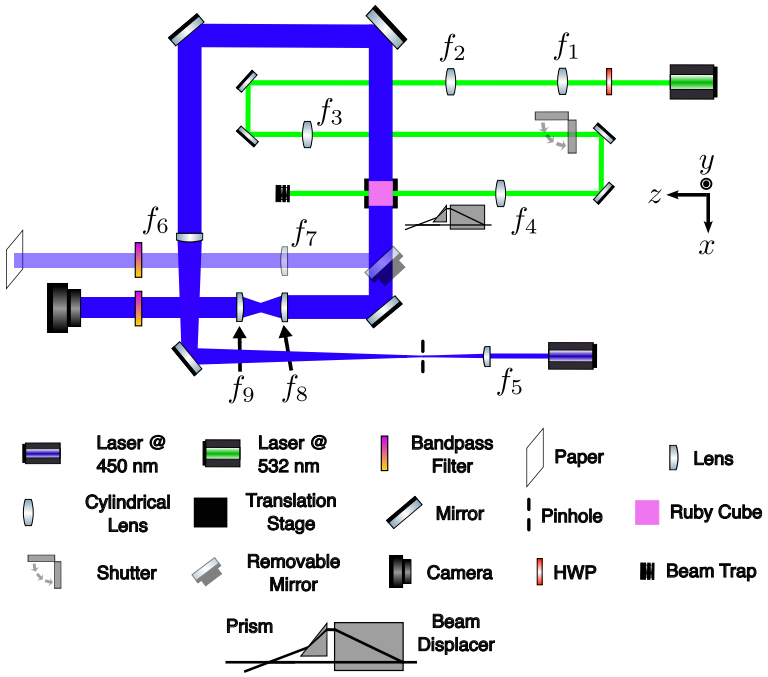

Fig. S1. Complete Experimental Setup. The setup of Fig. 2 (C) of the main article is expanded upon to include additional elements.

3. EXPERIMENTAL SETUP IN DETAIL

All images in Figure 1 of the main text were taken using an Olympus OM-D EM-5 Mark II with a M. Zuiko 17mm f/1.8 prime lens. Fig. S1 gives further information about the experimental setup. The illumination laser is a 450 nm 4.5 mW diode blue laser. The optical power which covered the face of the ruby is 285.06 μW. The object laser is a *Millennia eV* 532 nm CW laser, whose optical power output is adjustable and is in the TEM_{00} spatial mode. This laser is shaped into an ellipse stretched in the x dimension using two pairs of cylindrical lenses. The first pair ($f_1 = 100$ mm, $f_2 = 400$ mm) stretches the beam in the x dimension and the second pair ($f_3 = 500$ mm, $f_4 = 50$ mm) squeezes in y. The other lenses in the setup are: $f_5 = 45$ mm, $f_6 = 1000$ mm, $f_7 = 125$ mm, $f_8 = 300$ mm, and $f_9 = 50$ mm. The bandpass filter used was a 450 ± 8 nm CWL, 40 ± 8 nm FWHM filter. The same filter is used in the CMOS images, as well as in the photography camera images, just moved from one optical path to the other.

4. TEMPERATURE DEPENDENCE

Variations in temperature change the optical properties of ruby, as previously studied in Ref. [3]. In our experiment, the presence of the green object laser can significantly increase the temperature of the ruby crystal. This causes a reduction in the observed contrast of the laser shadow, as seen in Fig. S2. Furthermore, this also causes the contrast to have a nonlinear relationship as a function of input power, which goes against our model. For these reasons, we used a shutter in the green laser's path to limit the amount of time the ruby will be exposed to intense light, reducing the overall temperature effects. The shutter was set such that it exposes the ruby to the green object laser for ≈ 500 ms. Once a full dataset was obtained, the ruby is allowed to cool down to room temperature (23 °C) before the next dataset is collected. All data presented in our quantitative analysis as reported in Fig. 3 (B) and (C) of the main article were taken using this control mechanism.

For the nonlinear behavior of Fig. S2, our hypothesis is that the heating of the ruby cube affects the populations of the atomic levels, so that the effect as described in section Theory is impaired, leading to a reduction in the contrast. Table S1 reports the measured temperatures both with and without the shutter, demonstrating the large temperature difference observed.

5. ATTENUATION COEFFICIENT

We report in Table S2 the attenuation coefficient α, mathematically defined in Eq. S7, as the illuminating laser beam travels through the object laser beam for different optical powers of the object laser beam.

6. LASER SHADOW VIDEO

We included in the supplement a short real-time video (mp4 format) in which one can see the laser shadow moving as the prism in the object laser beam (green) path was being manually tilted. This video was recorded with object laser beam (green) set to 20 W of optical power.

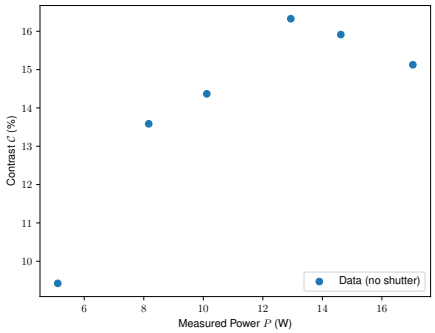

Fig. S2. Shadow contrast affected by temperature. This graph shows the measured shadow contrasts for varying green laser optical power in the ruby cube when data was taken without the shutter (i.e., without temperature control).

Nominal Power (W)	Temperature (°C) Without Shutter	Temperature (°C) With Shutter
5	63	26
8	82	28
10	96	29
13	112	31
15	124	32
18	137	34

Table S1. Power vs. Temperature. Measurements of the temperature of ruby cube with and without the temperature control for different nominal power values of the object laser beam (green).

Nominal Power (W)	Attenuation coefficient α (m^{-1})
5	133.5
8	144.9
10	151.8
13	161.1
15	166.3
18	173.6

Table S2. Attenuation coefficient. Attenuation coefficient as the illuminating laser beam (blue) travels through the object laser beam (green) for different nominal power values of the object laser beam (green).

REFERENCES

1. D. Cronemeyer, "Optical absorption characteristics of pink ruby," JOSA **56**, 1703–1705 (1966).
2. J. W. Huang and H. W. Moos, "Absorption Spectrum of Optically Pumped Al_2 O_3:Cr^{3+}," Phys. Rev. **173**, 440–444 (1968).
3. Y. Kiang, J. Stephany, and F. Unterleitner, "Visible spectrum absorption cross section of Cr^{3+} in the ^{2}E state of pink ruby," IEEE J. Quantum Electron. **1**, 295–298 (1965).